THIN TAPE TRACTION OVER A GROOVED ROLLER

By

Tugce Kasikci and Sinan Müftü
Northeastern University
USA

ABSTRACT

Traction between a thin, O(5 μm), tensioned tape and a grooved roller is studied. In the slow tape speed limit, tape contact over a grooved roller is studied analytically. A closed form relationship for the belt-wrap formula for grooved rollers is developed. In this range, air lubrication effects can be negligible and tape-to-roller contact is dominated by tape deflection in the lateral direction. At operational tape transport speeds, O(1-5 m/s), a relatively wide range of design parameters (groove width, land width) and device parameters (velocity and tension) were used to characterize the traction of a thin tape over a grooved roller. It was shown that air lubrication effects reduce the contact force, however the underlying effects of tape mechanics are not entirely eliminated. This work contributes to our understanding of traction mechanics of thin webs over grooved rollers, which has been understudied in the past, and helps in selecting design parameters for improved traction.

NOMENCLATURE

Greek:

μ_s	static friction coefficient
μ_e	effective static friction coefficient
∇^4	biharmonic derivative operator
δ	guide shape
λ_a	molecular mean free path
μ	viscosity of air
Δx	size of mesh in x-direction
Δy	size of mesh in y-direction
Δt	time step size
$\delta_x(x)$	guide shape variation in running direction
$\delta_y(y)$	guide (groove) shape variation in lateral direction
σ	asperity engagement height

Roman:

A_c	apparent contact area
c	tape thickness
D	tape bending rigidity
D_s	shell stiffness
$D(\ )/Dt$	material time derivative
E	elastic modulus
H	Heaviside step function
h	tape-to-roller spacing
$2L_G$	groove width
$2L_L$	land width
L_x	tape length
L_y	tape width
L_1, L_2	tangency points of the tape
p	air pressure
p_c	contact pressure
P_o	asperity compliance parameter
q	total contact force per unit circumferential length
$R(x)$	tape radius of curvature
R_g	roller radius
ρ	mass density
T	tape tension
v	Poisson's ratio
V_c	corner shear force
V_i	inner shear force
V_t	Tape speed
V_r	Roller speed
w	out of plane tape deflection
x	longitudinal coordinate direction
y	lateral coordinate direction

INTRODUCTION

Cylindrical rollers are often used as guiding and supporting elements in tape recording and web-handling applications. It is crucial for the tape[1] to remain in contact with its supporting rollers in order for it to follow a designated path. Traction capability of a roller is compromised when air creates a lubrication layer in the tape-roller interface [1].

The no-slip condition between air and a translating tape causes air to enter and lubricate tape-to-guide interface. Surface of a spinning roller exacerbates this problem. It has been shown experimentally and theoretically that the air pressure that develops under the foil is closely coupled to foil (tape, web) deflections. Mechanics of the *foil bearing* problem has been investigated analytically [6, 7] and numerically [8-14] among many.

Under negligible air lubrication, tape-to-roller contact pressure, p_c, is equal to the *belt-wrap pressure*, T/R_gL_y, where T is tape tension, L_y is tape width and R_g is roller radius. It is generally understood that due to rough nature of the surfaces, contact takes place on the summits of the asperities, leaving some open volume in which air can flow.

[1] The problem analyzed in this paper is motivated by tape recording therefore the term tape will be used instead of web throughout this paper.

Air pressure p increases with increasing tape speed and eventually provides another mechanism to support the belt-wrap pressure. Combined effects of air and contact pressures at sufficiently high tape velocities balance belt-wrap pressure. Rice et al. investigated web-to-roller contact in view of air entrainment, experimentally and numerically for non-grooved rollers [1]. Müftü and Jagodnik presented a non-dimensional model of traction between a web and a non-grooved roller [13].

Assuming that *transfer of shear stress transfer between the tape and the roller*, or *traction*, is governed by Coulomb's friction law, it can easily be seen that increasing air pressure would reduce the amount of contact pressure required to provide balance the belt wrap pressure. Consequently, the frictional force required to sustain high traction can be effectively reduced, without altering the value of the coefficient of static friction, μ_s. An *effective static friction coefficient* μ_e is defined by using the proportion of the computed contact force to belt-wrap force [1],

$$\mu_e = \mu_s \frac{RL_y}{TA_c} \int_{A_c} p_c dA \qquad \{1\}$$

where A_c is the *apparent contact area*. Effective friction coefficient is an indication of how much shear stress can be transferred between the two surfaces without inducing slip or *traction-loss*. In this work we compute the μ_e/μ_s ratio, where the values of 1 and 0 indicate no-loss and full-loss of traction, respectively.

Often grooves are manufactured on the roller surface in order to reduce the air lubrication effects [2-5]. Ducotey and Good numerically studied optimal groove geometry for grooved rollers [2]. They focused on rollers with circumferentially oriented grooves with rectangular cross-sections. They showed that contact becomes more reliable, and traction loss is reduced with increasing groove pitch and groove depth. Tran et al. presented a numerical model to analyze the fluid-structure interactions between a web and a spirally-grooved roller [14]. Their study included the dynamics effects that occur on spirally grooved rollers, and experiments confirmed their model. Rice and Gans presented a model where they considered the loss of wrap due to the air entrainment [1, 4, 5]. They assumed that the web is rigid in the lateral direction, and has zero bending stiffness. They developed a closed form relationship for traction loss as a function of roller radius, land and groove widths, static friction coefficient, upstream tape tension, tape speed and surface asperity height. They carried out traction experiments with different grooved roller shapes. Their study is applicable to relatively thick webs.

Traction of thin tape over a grooved roller is investigated in this paper. Effects of tape deflection in the lateral direction as well as air lubrication are considered.

THEORY

Tape is modeled as a tensioned, translating shell (Figure 1) while effects of air lubrication are modeled by using the Reynolds equation. Tape-to-roller contact is modeled by using a non-linear contact pressure function. Both governing equations are expressed in their transient forms, and solution is obtained by using a fully transient coupling algorithm [4].

Equation of motion of the out-of-plane tape deflection, w, is represented as a tensioned, translating shell as follows [15, 16, 11],

$$\rho\frac{D^2w}{Dt^2}+D\nabla^4w-\frac{T}{L_y}w_{,xx}+D_sw=p+p_c-\frac{T}{L_yR} \quad \{2\}$$

where ρ is mass density, T is tension, D is bending rigidity of the tape, and x and y are the longitudinal and lateral coordinate directions, respectively (Figure 1), L_x is tape length between the supports, L_y is tape width. $D(\ )/Dt$ represents the material time derivative. ∇^4 represents the bi-harmonic derivative operator. The shell stiffness of the tape is $D_s = Ec/R^2(1-\nu^2)$ with elastic modulus E, Poisson's ratio ν and thickness c of the tape. Tape radius is defined as follows,

$$R(x)=R_g\left(H(x-L_1)-H(x-L_2)\right) \quad \{3\}$$

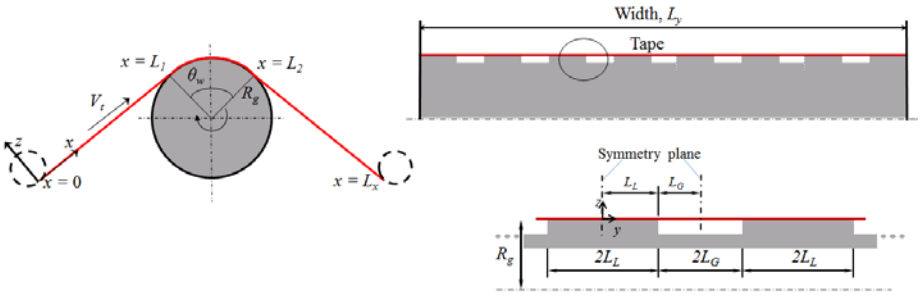

Figure 1 − Schematic cross-section of a grooved roller and details of the area considered in analysis.

where R_g is the roller radius, H is the Heaviside step function, and L_1 and L_2 are the tangency points of the tape (Figure 1). The contact pressure p_c is given as follows [9,11],

$$p_c=P_o\left(1-\frac{h}{\sigma}\right)^2\ \left(1-H(h-\sigma)\right) \quad \{4\}$$

where P_o is the is asperity compliance and σ is asperity engagement height. The tape-to-roller clearance, h, is found as follows,

$$h=w+\delta \quad \{5\}$$

where guide shape, δ, is defined by superposition of two functions as follows,

$$\delta(x,y)=\delta_x(x)+\delta_y(y) \quad \{6\}$$

The functions $\delta_x(x)$ and $\delta_y(x)$ describe the guide shape variations in the running and lateral directions, respectively. The groove shapes are introduced by $\delta_y(y)$ as shown in Figures 1 and 2, and characterized by the variables; *groove width*, $2L_G$, and *land width*, $2L_L$. The grooves are assumed to be sufficiently deep to validate the assumption of ambient pressure over them.

Only one land and the two grooves around the land are included in the coupled simulations. Symmetry conditions around a single land are used along the lateral edges of the tape,

$$\frac{dw}{dy} = V_y = 0 \quad \text{along } 0 \le x \le L_x, \text{ and } y = \pm\left(L_G + L_L\right) \qquad \{7\}$$

Longitudinal edges of the tape are simply supported,

$$w = \frac{d^2 w}{dx^2} = 0 \text{ at } x = 0, L_x \text{ and along } -\left(L_G + L_L\right) \le y \le \left(L_G + L_L\right) \qquad \{8\}$$

Air pressure, p, is generated by air lubrication which is governed by the compressible Reynolds lubrication equation, with slip flow corrections given as follows [11],

$$\frac{\partial}{\partial x}\left[h^3 p \frac{\partial p}{\partial x}\left(1 + 6\frac{\lambda_a}{h}\right)\right] + \frac{\partial}{\partial y}\left[h^3 p \frac{\partial p}{\partial y}\left(1 + 6\frac{\lambda_a}{h}\right)\right] = 6\mu\left(2\frac{\partial ph}{\partial t} + \left(V_t + V_r\right)\frac{\partial ph}{\partial x}\right) \qquad \{9\}$$

where λ_a is molecular mean free path, μ is viscosity of air. In this work the air pressure is computed only over the lands. Therefore, the air pressure is ambient around the periphery of the lands and along the outer edges of the tape. The dependent variables w, p and p_c are found by the coupled solution of equations (2) – (8) [11].

As it is demonstrated later in the paper it is instructive to separate the effects of contact and air lubrication. An analytical solution can be obtained to predict the contact states of a tape wrapped around a grooved roller by assuming air lubrication effects are negligible. This of course happens when the system is tensioned but stationary. The problem can be reduced to a one-dimensional problem by making the following additional assumptions:

i) contact-surface of the roller consists of circumferentially oriented lands separated by grooves; *ii*) lands are flat and parallel to the roller axis; *iii*) tape is wrapped around the roller with a sufficiently large wrap-angle. Tape-to-roller contact problem in this case can be reduced to analyzing the contact mechanics of a single groove-land pair as described in Figure 2. For the assumptions listed above, tape deflections can be assumed to be independent of the circumferential direction and equation {2} becomes,

$$Dw_{,yyyy} + D_s w = p_c - \frac{T}{R_g L_y} \qquad \{10\}$$

Shell stiffness D_s and belt-wrap pressure (T/R_gL_y) originate from the hoop strain (w/R_g) and initial tension in the material, respectively [15]. While the belt-wrap pressure provides a constant pull over the cylindrical guide, the hoop strain provides a resistance that is proportional to deflection, w. Thus in equation{10} the effect of hoop strain appears similar to a linear-elastic foundation force.

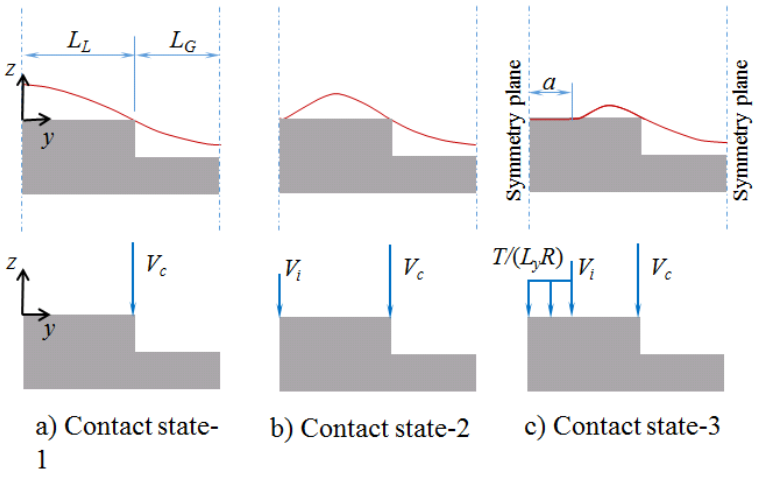

Figure 2 − Description of the three possible contact states when the tape is "pushed" against the grooved roller by the belt-wrap pressure.

In a recent study the authors have shown that three distinct *contact states*, depicted in Figure 2, are possible depending on the parameters of the problem [17]. In all of these states the belt wrap pressure pushes the tape to bend into the grooves, and the tape deflects away from the land. In *contact state*-1 (CS) tape makes contact only along the edge ($y = L_L$) of the land. In *contact state*-2 (CS-2) tape makes contact along the edge and the center ($y = 0$) of the land. In *contact state*-3 (CS) the central contact on the lands spreads to a finite contact area of width a, while edge contact is maintained. Tape deflection profile over the land, $w^{(1)}(y)$, and the groove, $w^{(2)}(y)$, are obtained from Equation {1}, with the appropriate boundary conditions presented in reference [17]. For a given set of parameters, it is not clear a priori which one of the contact states will be established. Therefore, the problem is non-linear and is solved by using a semi-analytic approach [17].

Tape Parameters		Air Parameters	
E (GPa)	9	μ (Pa*s)	1.81×10^{-5}
ν	0.3	λ_a (m)	6.35×10^{-8}
ρ (kg/m^3)	3000	Contact Parameters	
c (μm)	6.4	σ (nm)	90
L_y (mm)	12.7	P_o (Pa)	100
L_x (mm)	7.23		
T (N)	0.3, 0.5, 0.7		
Roller Parameters		Numerical Parameters	
R_g (mm)	7.615	Δx (μm)	9.028
$2L_L$ (μm)	150, 300, 450	Δy (μm)	9.028
$2L_G$ (μm)	150, 300, 450	Δt (ns)	5

Table 1 – Parameters used in this study.

In all three contact states described above, tape contacts corners of the land. The distributed contact force that is associated with contact along the corner of the land is equal to the jump in the shear force resultant as follows,

$$V_c = -D\left(w^{(2)}_{,yyy} - w^{(1)}_{,yyy}\right)_{y=L_L} \qquad \{11\}$$

In contact state-3, the tape contacts the center of the land and the resulting contact pressure is given by the following relationship,

$$p_c = \frac{T}{R_g L_y} \quad \text{for} \quad 0 \le y \le a \qquad \{12\}$$

In addition, a concentrated force develops along the edge of the inner contact region for both contact states-2 and -3. These are defined as follows,

$$V_i(0) = -D^{(1)}_{,yyy}(0) \text{ for CS-2 (a)} \quad \text{and} \quad V_i(a) = -D^{(1)}_{,yyy}(a) \text{ for CS-3 (b)} \qquad \{13\}$$

Contact force per the unit circumferential length, for the symmetric problem described by the three contact states can therefore be summarized as follows,

$$q = \begin{cases} V_c, & \text{for CS-1} \\ V_c + V_i(0), & \text{for CS-2} \\ V_c + V_i(a) + \dfrac{Ta}{R_g L_y}, & \text{for CS-3} \end{cases} \qquad \{14\}$$

Total contact force per unit circumferential length then becomes, $q = N_p q$ where $N_p = L_y / 2(L_L + L_G)$ is the number of land-groove pairs along the roller. Note that the effects of the free lateral edges of the tape are neglected in equation {14}.

RESULTS AND DISCUSSION

Figure 3 shows the contact states for different land and groove width combinations under different tension values in case the air lubrication effects are negligible. Each row on the graph corresponds to a different land width. First, second and third rows correspond to $2L_L$ = 150, 300 and 450 μm, respectively. Similarly, the columns represent three different groove widths $2L_G$ = 150, 300 and 450 μm. Thus, each graph on the matrix represents a specific combination of land and groove widths. The authors recently reported that the contact states described above depend mainly on the land and groove widths; and, tension only adjusts the displacement amplitude within a contact state [17].

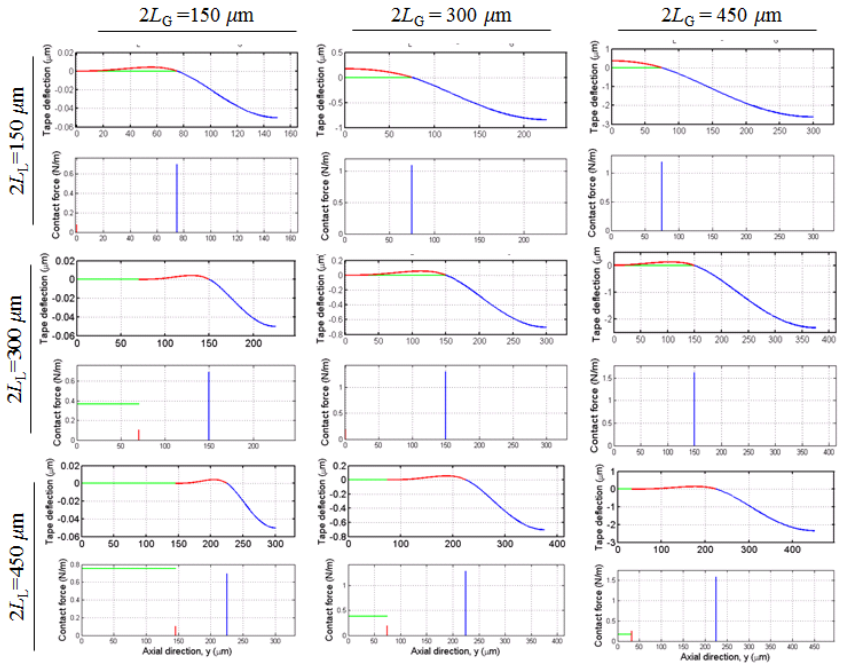

Figure 3 – Variation of tape deflection and contact force predicted by closed form analysis for T = 0.5 N and different land and groove width combinations.

This behavior is attributed to the competition between the moment resultants due to belt wrap pressure acting over the land and groove regions. This can be seen when Figure 3 is investigated row-by-row. The first row of this figure corresponds to $2L_L$ = 150 μm. Increasing the groove width from 150 μm to 450 μm (left to right) increases the resultant moment from the groove region while the resultant moment from the land region remains constant. As a result, the tape deflection transitions from CS-2 at $2L_G$ = 150 μm to CS-1 at $2L_G$ = 300 and 450 μm. Increasing, tension only scales the displacement amplitudes, as expected and demonstrated in reference [17].

In the second row of Figure 3, the land width is $2L_L$ = 300 μm. Therefore, the resultant moment due to belt wrap pressure acting over the land has a larger contribution. In fact, for $2L_G$ = 150 μm, the tape makes contact along the center of the land (CS-3). Increasing the groove width to 300 and 450 μm increases the corresponding moment contribution, but the tape primarily bends toward the land.

In the final row of Figure 3, the land width is $2L_L$ = 450 μm. As expected, based on the descriptions given above, the resultant moment due to belt wrap pressure over the groove is not sufficient to "pop" the tape away from the land, and the tape remains in contact state-3 for all three cases ($2L_G$ = 150 – 450 μm).

The effects of air lubrication are evaluated for V_t = 0.5 – 6 m/s and T= 0.5 N in Figures 4 – 6 with the same geometry and tension values. This analysis is performed by the coupled solution method described previously. Figure 4 shows the cross-sections of the tape deflection profiles along the lateral direction, at the center of the wrap, whereas Figures 5 and 6 show air and contact pressure distributions over a single land for different parameters.

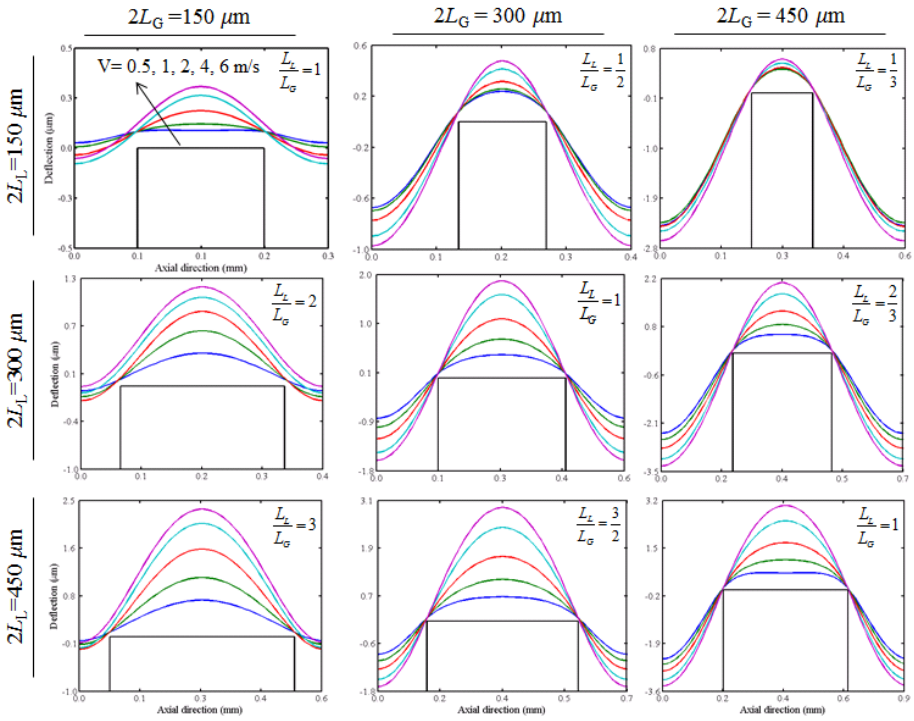

Figure 4 – Lateral cross-sections of tape deflection at center of wrap, predicted by coupled air-tape deflection analysis for T = 0.5 N and different land and groove widths.

Results presented in Figure 4 can be compared directly with those presented in Figure 3. In general, it is seen tape deflection over the land increases with speed. This effect is due to increasing air pressure. This figure also shows no central contact with the lands, as it was observed in dry contact cases.

Figure 4 also shows that while tape deflection depends on tape velocity it is also influenced significantly by the land and groove width values. For example, the tape behaves considerably stiffer with increasing tape speed for ($2L_L$, $2L_G$) combinations of (150, 300) μm and (150, 450) μm. Note that the analysis presented in Figure 3 showed that these two cases are expected to remain in contact state-1, and they are dominated by the belt wrap pressure acting over the groove. Thus even for the stationary tape (V_t = 0) a "cupped" shape appears in the tape-land interface. This built-in clearance reduces the effects of air lubrication, and the air pressure does not couple to tape deflection as in the classical foil bearing. This can be seen in the air pressure distributions presented in Figure 5 for ($2L_L$, $2L_G$) = (150, 450) μm. In particular, for V_t = 0.5 and 2 m/s relatively low and non-characteristic air pressure distributions are predicted in the interface.

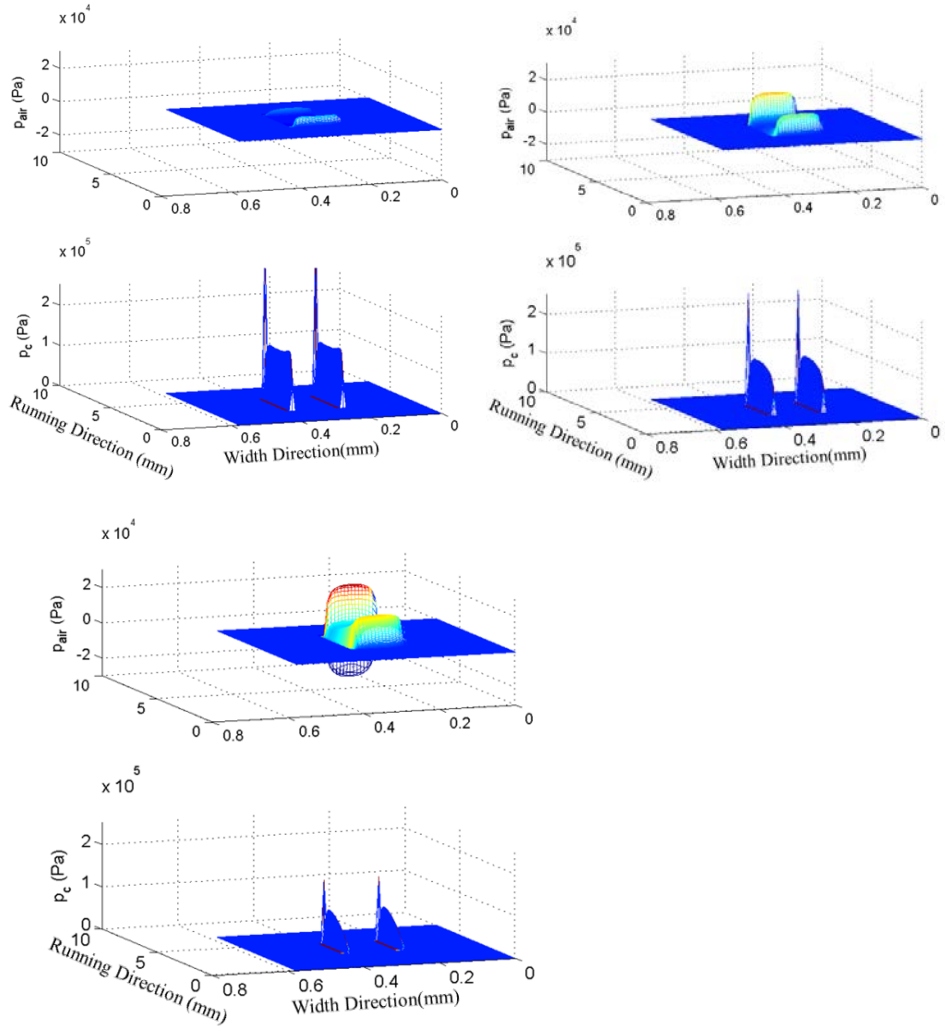

Figure 5 – Contact p_c and air pressure p variations for tension T = 0.5 N, land width $2L_L$ =150 μm and groove width $2L_G$ = 450 μm, tape speeds a) 0.5 m/s, b) 2 m/s, c) 6 m/s.

For all other cases, where the land width, $2L_L$, is high and the ratio L_L/L_G is greater than one, the initial gap over the land caused by the belt wrap pressure at zero tape velocity is much lower (Figure 3). In these cases, air lubrication and tape deflections couple much more easily. When $V_t > 0$, the air pressure and tape deflection find higher values.

Figure 6 shows air and contact pressure distributions for ($2L_L$, $2L_G$) = (450, 150) μm. In this case it is seen that air pressure is evenly distributed in most of the interface, and its amplitude increases gradually with tape speed from V_t = 0.5 m/s to V_t = 6 m/s. For this case the zero velocity analysis (Figure 3) shows that tape would be expected to contact the middle of the land. This supports the assertion that if tape makes contact with the land at zero tape speed, the coupling between the tape and the air lubrication is stronger, resulting in lifting of the tape and widening of the tape-land clearance.

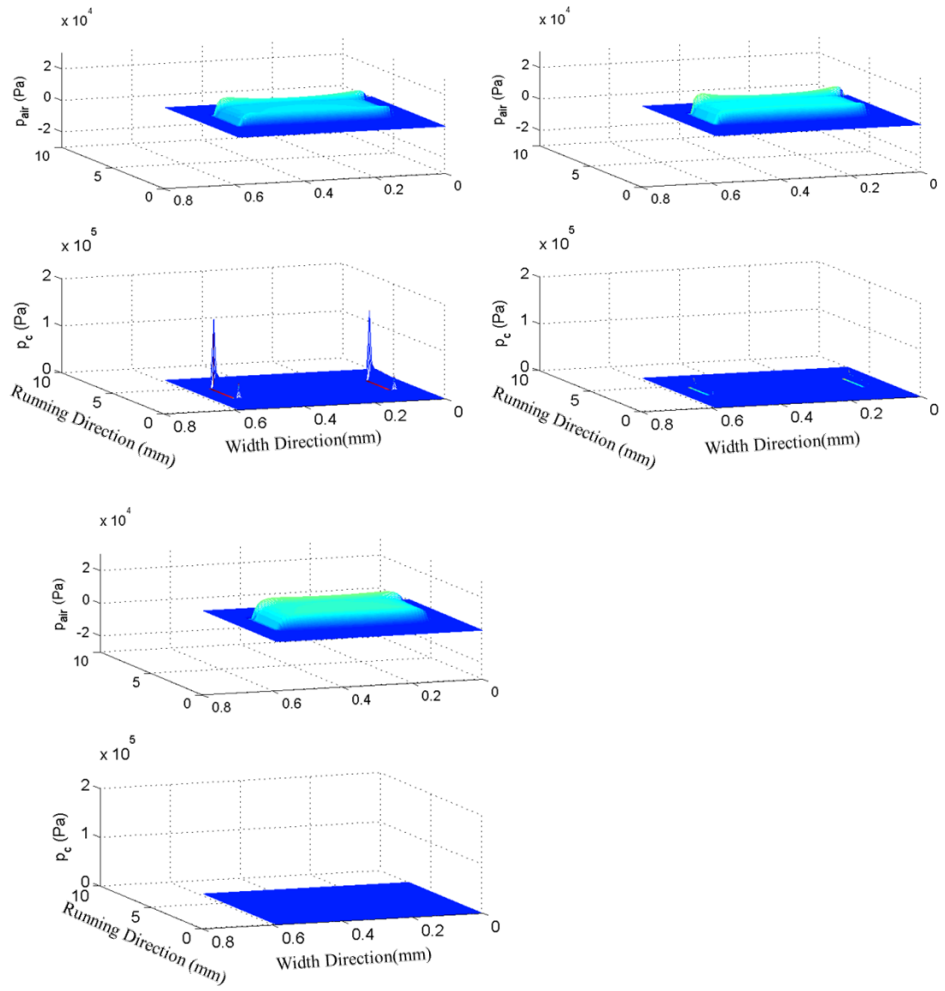

Figure 6 – Contact p_c and air pressure p variations for tension T = 0.5 N, land width $2L_L$ =450 μm and groove width $2L_G$ = 150 μm, tape speeds a) 0.5 m/s, b) 2 m/s, c) 6 m/s.

Figures 5 and 6 indicate that regardless of the of coupling level between the tape deflection and air pressure, increasing tape speed causes the contact pressure to decrease. In case of Figure 5, where ($2L_L$, $2L_G$) = (150, 450) μm non-negligible contact pressure along the edges of the lands remain even at 6 m/s tape speed. On the other hand, in Figure 6, contact pressure magnitude is reduced very drastically with speed such that all contact is lost at V_t = 6 m/s. This trend would have a strong influence on the traction capability.

Traction coefficients for all the cases presented above are computed as described by Equation {1} as functions of tape speed and tension. Traction coefficients computed in this work, as well as the predictions given by Rice and Gans [4] for the same parameters are presented by broken lines in Figure 7. Plots are arranged in the same order as in Figure 3. Note that the bending index given by Rice and Gans is much larger than the value that makes their analysis applicable for the cases considered in this paper and presented here without a level of high expectation.

Figure 7 shows that, in general, increasing tape speed and decreasing tape tension results in reduction of the traction coefficient as expected. Distinct differences are noticeable in the two cases where the deflection is governed by the tape bending ($2L_L$, $2L_G$) = (150, 300) and (150, 450) μm, where relatively less traction loss occurs with increasing speed. For the other combinations of ($2L_L$, $2L_G$) traction loss with tape speed is fairly large. In particular, more traction loss is predicted for the same speed and tension values with increasing L_L and L_L/L_G ratios.

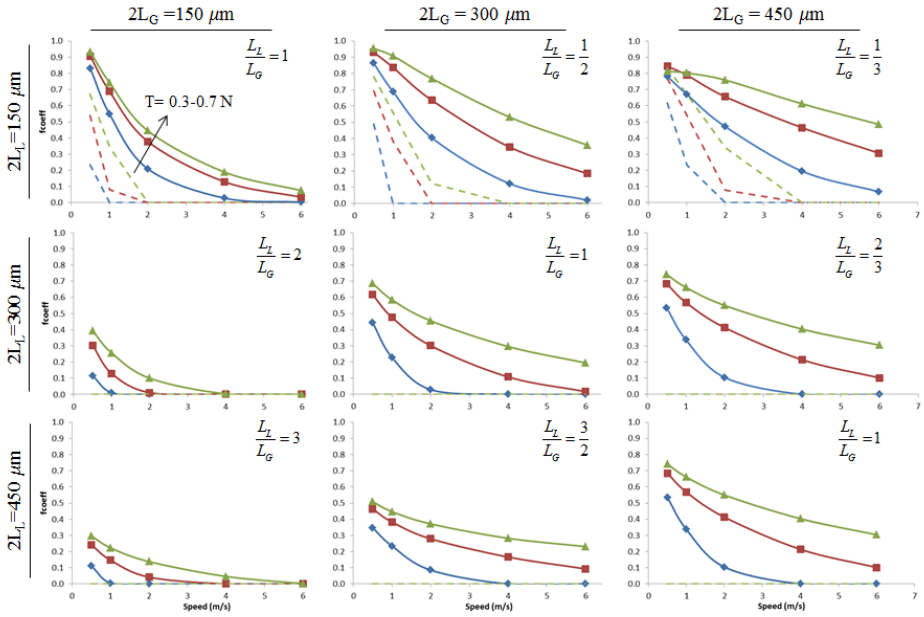

Figure 7 – Traction coefficient for land width $2L_L$ and groove width $2L_G$ combinations for all tension values. Blue lines represent T=0.3 N, red lines represent T=0.5 N and green lines represent T=0.7 N.

SUMMARY AND CONCLUSIONS

Traction between a thin, tensioned tape and a grooved roller is studied. In the slow tape speed limit an analytical approach can be described to model tape contact with a grooved roller. In this range, air lubrication effects can be negligible and tape-to-roller contact is dominated by tape deflection in the lateral direction. This is in contrast to previous work where tape bending in the lateral direction is neglected for much thicker webs. At operational tape transport speeds a wide range of groove width, land width, tape velocity and tension were used to characterize the traction of a thin tape over a grooved roller. It was shown that air lubrication effects reduce the contact force, however the underlying effects of tape mechanics are not entirely eliminated. In particular, it is shown that traction loss is worse for rollers with wide lands and narrow grooves. By using the principles described in this paper, it should be possible to design land and groove widths that are relatively insensitive to tape velocity.

ACKNOWLEDGEMENTS

The authors would like to acknowledge the partial funding provided by the International Storage Industry Consortium (INSIC) and Oracle Corporation, and the in-kind support of IBM-Zurich Research Laboratories and Quantum Corporation.

REFERENCES

1. Rice, B. S., Cole, K. A., and Müftü, S., "A Model for Determining the Asperity Engagement Height in Relation to Web Traction Over Non-Vented Rollers," Journal of Tribology, Vol. 15, No. 3, 2002, p. 584.
2. Ducotey, K. S., and Good, J. K., "A Numerical Algorithm for Determining the Traction between a Web and a Circumferentially Grooved Roller," Journal of Tribology, Vol. 122, No. 1, 2000, pp. 578-584.
3. Hashimoto, H., and Nakagawa, H., "Improvement of Web Spacing and Friction Characteristics by Two Types of Stationary Guides," Journal of Tribology, Vol. 123, No. 3, 2001, p. 509.
4. Rice, B. S., and Gans, R. F., "Predictive Models of Web-to-Roller Traction," Journal of Tribology, Vol. 127, No. 1, 2005, pp. 180-189.
5. Rice, B. S., and Gans, R. F., "A Simple Model to Predict Web-to-Roller Traction," Proceedings of the Seventh International Conference on Web Handling, 2003.
6. Barlow, E. J., "Derivation of Governing Equations for Self-Acting Foil Bearings," Journal of Lubrication Technology, July, 1967, pp. 334-340.
7. Eshel, A., and Elrod, H.G., Jr., "The Theory of the Infinitely Wide, Perfectly Flexible, Self-Acting Foil Bearing," Journal of Basic Engineering, December, 1965, pp. 831-836.
8. Stahl, K.J., White, J., and Deckert, K.L., "Dynamic Response of Self-Acting Foil Bearings," IBM Journal of Research and Development, Vol. 18, 1974, p. 513.
9. Lacey, C., and Talke, F. E., "A Tightly Coupled Numerical Foil Bearing Solution," IEEE Transactions on Magnetics, Vol. 26, 1990, pp. 3039-3043.
10. Rongen, P. M. J., "On Numerical Solutions of the Instationary 2D Foil Bearing Problem," American Society of Lubrication Engineers, Special Publication-29, 1990, pp. 130-138.
11. Müftü, S., and Benson, R. C., "A Study of Cross-Width Variations in the Two-Dimensional Foil Bearing Problem," Journal of Tribology, Vol. 118, No. 1, 1996, pp. 407-414.
12. Müftü, S., and Altan, M. C., "Mechanics of a Porous Web Moving over a Rigid Guide," Journal of Tribology, Vol. 122, 2000, pp. 418-426.
13. Müftü, S., and Jagodnik, J. J., "Traction between a Web and a Smooth Roller," Journal of Tribology, Vol. 126, No. 1, 2004, pp. 177-184.
14. Tran, S. B. Q., Yoo, Y. H., Ko, J. H., Kim, J., Byun, D., Lee, J. W., Byun, Y. H., and Shin, K. H. , "Experimental and Numerical Study of Air Entrainment Between Web and Spirally Grooved Roller," Journal of Tribology, Vol. 131, No. 2, 2009, pp. 1-8.
15. Müftü, S., and Cole, K. A., "The Fluid-Structure Interaction in Supporting Thin Flexible Cylindrical Web with an Air Cushion," Journal of Fluids and Structures, Vol. 13, No. 1, 1999, pp. 681-708.
16. Müftü, S., "Mechanics of a Thin, Tensioned Shell, Wrapped Helically around a Turn-bar," Journal of Fluids and Structures, Vol. 23, No. 5, 2007, pp. 767-785.

17. Kasikci, T., and Müftü, S., "Wrap Pressure between a Flexible Web and a Circumferentially Grooved Cylindrical Guide," Journal of Tribology, in review, April 2015.
18. Kasikci, T., and Müftü, S., "Modeling the Traction of a Thin Tape Guided by a Grooved Roller," Proceedings of the 23rd Annual Conference on Information Storage and Processing Systems ISPS2013, June 24-25, 2013, Santa Clara, California, USA.
19. Kasikci, T., and Müftü, S., "Tape Mechanics over a Grooved Roller: Experiments and Theory," Proceedings of the 24th Annual Conference on Information Storage and Processing Systems ISPS2014, June 16-17, 2014, Santa Clara, California, USA.